Quantitative Analysis of the Choriocapillaris in Uveitis Using En Face Swept-Source Optical Coherence Tomography Angiography

ZHONGDI CHU, JESSICA E. WEINSTEIN, RUIKANG K. WANG, AND KATHRYN L. PEPPLE

• PURPOSE: To perform a quantitative analysis of choriocapillaris (CC) flow deficits (FDs) in patients with uveitis.

• DESIGN: Retrospective cross-sectional study.

• METHODS: Swept-source optical coherence tomography based angiography (SS-OCTA) macular volume scans (3 × 3 mm and 6 × 6 mm) were obtained using the Plex Elite 9000. En face CC images were generated and analyzed using an automated FD identification algorithm. Three quantitative metrics were determined for each eye: FD number (FDN), mean FD size (MFDS), and FD density (FDD). Quantitative metrics were compared between uveitis and control eyes. The uveitis cohort was further subdivided by the presence or absence of choroidal involvement, and quantitative metrics were compared between subgroups and normal control subjects.

• RESULTS: A total of 38 eyes from 38 control subjects and 73 eyes from 73 uveitis subjects were included in this study. Eyes with uveitis have significantly larger CC MFDS (3- × 3-mm scans; $P < .0001$; 6- × 6-mm scans; $P < .0001$) and higher FDD ($P = .0002$; $P = .0076$, respectively) compared to control eyes. Additional analysis determined that these differences were due to the choroidal disease subgroup, which demonstrates significantly larger MFDS (3 × 3 = 1,108 μm^2; 6 × 6 = 1,104 μm^2) compared to both normal control eyes (752 μm^2; $P < .0001$; 802 μm^2; $P < .0001$, respectively) and uveitis patients without choroidal involvement (785 μm^2; $P < .0001$; 821 μm^2; $P < .0001$, respectively). No significant differences were found between the quantitative metrics of control subjects and patients without choroidal involvement.

• CONCLUSIONS: Automated quantification of CC can identify pathological FDs and provide quantitative metrics describing such lesions in patients with uveitis. Posterior uveitis patients have significantly larger CC FDs than patients with other forms of uveitis. (Am J Ophthalmol 2020;218:17–27. © 2020 Elsevier Inc. All rights reserved.)

Accepted for publication May 5, 2020.

From the Department of Bioengineering (Z.C., R.K.W.), University of Washington, Seattle, Washington, USA; and the Department of Ophthalmology (J.E.W., R.K.W., K.L.P.), University of Washington, Seattle, Washington, USA.

Inquiries to Kathryn L. Pepple, Box 359607, 325 Ninth Avenue, Seattle, Washington 98104, USA; e-mail: kpepple@uw.edu

OPTICAL COHERENCE TOMOGRAPHY ANGIOGraphy (OCTA) is a noninvasive imaging modality that has demonstrated utility in studies of retinal vasculature disease.[1–9] In patients with uveitis, including intermediate, posterior, and panuveitis, spectral domain OCTA (SD-OCTA) has identified both qualitative and quantitative retinal vascular flow abnormalities.[3,6,10–13] However, in certain types of uveitis, such as birdshot chorioretinopathy or punctate inner choroidopathy, pathology may also involve or be entirely limited to the choroid and choriocapillaris (CC).[3,6,10,14–18] Although case reports and case series using SD-OCTA have identified CC flow abnormalities in patients with some forms of posterior uveitis, the vascular beds below the retinal pigmented epithelium (RPE) complex have not been thoroughly investigated, and quantitative analysis of CC abnormalities is limited.[19–21]

The emergence of swept-source OCTA (SS-OCTA) technology allows for more in-depth characterization of choroidal blood flow in healthy and diseased eyes. SS-OCTA imaging can provide improved visualization of blood flow in the choroid and CC due to better depth penetration through the RPE/Bruch's membrane (BM) complex and lower sensitivity roll-off than SD-OCT systems.[22] Additionally, acquisition speeds of more than 100 kHz facilitate wide angle imaging,[23] a feature important for diseases such as uveitis that frequently manifest clinically significant lesions in the extrafoveal macula. Finally, segmentation of SS-OCTA data into choroidal or CC en face slabs is showing promise for the detection of inflammatory disease activity without a need for fluorescein or indocyanine green based angiography.[15,24–27] In order to bring these benefits of SS-OCTA imaging into more widespread clinical use, image acquisition will need to be coupled with automated image analysis for the rapid, reproducible, and quantitative detection of relevant disease associated abnormalities. This study tested an automated en face CC OCTA image analysis approach for the ability to detect and quantify CC in patients with uveitis.

SUBJECTS AND METHODS

THIS SINGLE-INSTITUTION RETROSPECTIVE CROSS-sectional study was approved by the Institutional Review

0002-9394/$36.00
https://doi.org/10.1016/j.ajo.2020.05.006

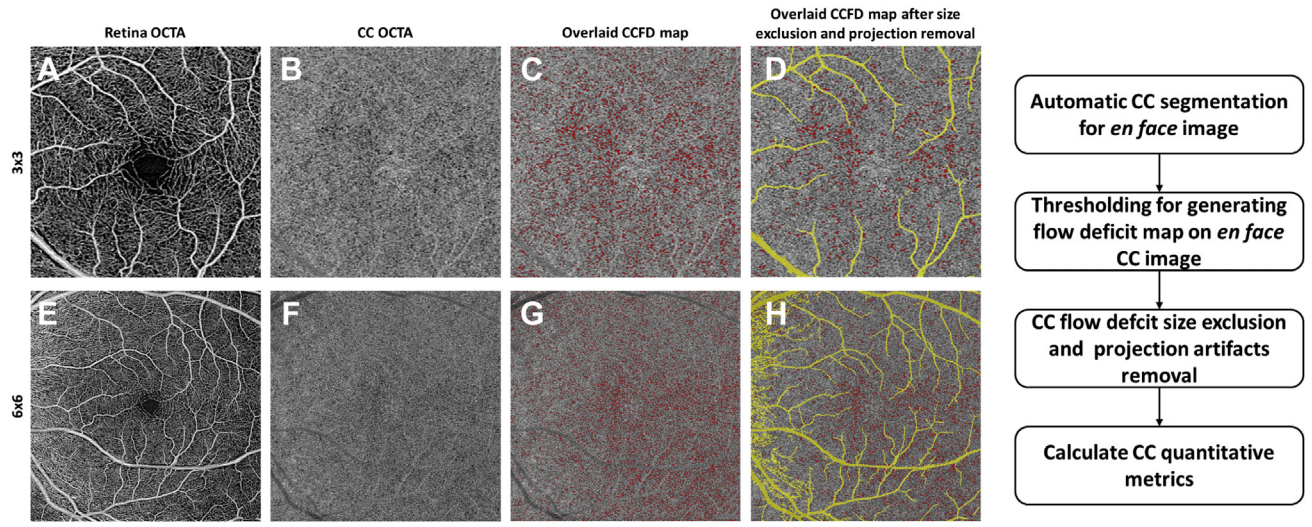

FIGURE 1. Automated detection and quantification of choriocapillaris (CC) flow deficits from en face swept-source optical coherence tomography angiography (OCTA) images. An example of the authors' proposed CC analysis in a normal patient using both 3- × 3-mm scans (A-D) and 6- × 6-mm scans (E-H). I = flow chart of the proposed CC analysis.

Board at the University of Washington. Written informed consent regarding the nature of this research study was obtained for all subjects before imaging. This study was performed in accordance with the tenets of the Declaration of Helsinki and the Health Insurance Portability and Accountability Act of 1996.

• **STUDY POPULATION:** Patients 18 years or older, with a diagnosis of anterior, intermediate, posterior, panuveitis, or retinal vasculitis were recruited for SS-OCTA imaging between August 2016 and July 2018 at the University of Washington Harborview Medical Center Eye Institute. Patients with active and inactive uveitis were recruited. Upon entry in the study, subject data including sex, age, uveitis diagnosis, and involvement of 1 or both eyes were collected. Anatomic location of uveitis and determination of location of disease activity were diagnosed by using the criteria established by the standardization of uveitis nomenclature criteria based on clinical examination and additional imaging modalities such as color fundus, fluorescein angiography, indocyanine green angiography, SD-OCT, and fundus autofluorescence at the discretion of the examining physician.[28] Results of laboratory testing, chest radiographs, biopsy, or magnetic resonance imaging, when performed, were used to further classify uveitis diagnosis by underlying cause.

• **IMAGE ACQUISITION AND SCANNING PROTOCOLS:** Research imaging was performed using a 100-kHz SS-OCTA Plex Elite 9000 (Carl Zeiss Meditec, Dublin, California), with a central wavelength of 1,060 nm, a bandwidth of 100 nm, an axial resolution of ~6 μm, and a lateral resolution of ~20 μm in retinal tissue.[29] FastTrac (Carl Zeiss Meditec, Dublin, California) motion tracking was used during all scans to minimize possible motion artifacts during imaging. Volume scans of 3 × 3 mm and 6 × 6 mm centered on the fovea were obtained for both eyes of all subjects. For unilateral cases, the diseased eye was selected for further analysis, and for bilateral cases, the eye with the highest signal strength was selected. If both eyes were equal in signal strength, then the right eye was used. Images with severe motion artifacts, macular edema, and signal strength lower than 7 were excluded from further analysis.[30]

The commercially available Plex Elite algorithm was used to segment the CC and generate en face CC flow images. Briefly, the RPE best fit line was determined using Plex Elite software, and manual corrections were performed in the case of failed automated segmentation. The CC was defined as the region from 16 to 31 μm below the RPE.[31] The complex optical microangiography (OMAG^c) algorithm[32] was used to generate OCTA volumes, and then maximum projection was applied to the segmented CC OCTA volumes to generate the en face images. After CC en face images were acquired, a previously published compensation strategy using structural OCT information was also applied using Matlab version R2016b software (MathWorks, Natick, Massachusetts) to correct the OCTA flow in the CC images for signal attenuation.[33] Quantitative analysis was then performed of the en face image.

• **DEFINITION AND QUANTIFICATION OF CC FD:** In this study the term *flow deficit* (FD) is used to describe areas where there is a lack of flow or the flow is below the detectable threshold of OCTA.[34,35] In normal control subjects, these areas are believed to represent the CC vascular walls and intercapillary spaces. In disease states, these areas are

TABLE 1. Patient Demographics

	Control	Uveitis		*P* Value
Number	38	73		NA
Mean ± SD age, y (range)	54 ± 22 (32-76)	49 ± 15 (22-75)		.221
Females	53%	71%		.057
Anatomic classification		Anterior	20	NA
		Intermediate	8	NA
		Posterior	40	NA
		Panuveitis	5	NA

NA = not applicable.

believed to represent choroidal perfusion or the presence of choroidal infiltrates leading to blood flow that is below the OCTA detection sensitivity. The similar term *flow void* has been used in other reports[36–38] and is well described in the medical literature.[39] FDs were defined on each en face image by using a customized algorithm through Matlab version R2016b (MathWorks), using a comprehensive thresholding strategy.[34] This method is summarized in Figure 1. Briefly, for each en face CC slab, a complex thresholding algorithm that used fuzzy C-means clustering was applied. Pixels that self-clustered into the lowest intensity group were segmented as the initial FDs. The image was then binarized such that areas of CC flow were bright, and the areas of absent flow (FDs) are dark (Figure 1, B and F). The final corrected FD map was generated after masking out areas of projection artifacts from overlying retinal vasculature[40] and removing FDs that were subphysiological in size (i.e., less than the normal intercapillary distance) (Figure 1, C and G).[34] Finally, quantitative analysis was performed using the corrected map.

Three quantitative metrics defined for each image were FD number (FDN), mean FD size (MFDS), and FD density (FDD) (Figure 1, J). FDN was defined as the total number of all individual FDs identified per image. MFDS was defined as the mean size (square micrometers [μm^2]) of all individual FDs identified per image. FDD was defined as the total area occupied by CC FDs-to-total image area ratio (minus projection artifacts).

• **DETERMINATION OF COEFFICIENT OF VARIATION:** Five control subjects and 5 subjects with posterior uveitis were scanned 3 times at the same visit by using both the 3- × 3-mm scans and the 6- × 6-mm scans. Three of the posterior uveitis patients had a diagnosis of birdshot chorioretinopathy, and the other two had a diagnosis of serpiginous choroiditis. Repeatability was calculated for each of the quantitative metrics, FDN, MFDS, and FDD, and reported as the coefficient of variation (CV).[41]

• **STATISTICAL ANALYSIS:** Statistical analyses were performed using Matlab R2016b software (MathWorks) and Prism software (GraphPad, San Diego, California). Cohort data were expressed as the median and interquartile range (IQR). The Mann-Whitney *U* test and Kruskal-Wallis test were used to compare control and uveitis cohorts; *P* values less than .05 were considered significant in the case of multiple comparisons; Bonferroni correction was performed such that *P* values less than .05/n were considered significant, where "n" was the number of comparisons made. Nonparametric Spearman correlation was used for correlation testing of groups with non-normal distributions. The receiver operating characteristic (ROC) curve was plotted, and the area under the curve (AUC) was calculated to compare the diagnostic power of each metric.

RESULTS

A TOTAL OF 78 UVEITIS SUBJECTS AND 38 CONTROL SUBjects were recruited and imaged. Five uveitic subjects were excluded, 3 because of the presence of macular edema and 2 because of insufficient scan quality. No control subjects were excluded. For the remaining subjects, both eyes of 73 uveitis patients and 38 control subjects were imaged and examined. One eye per subject was selected for further analysis as (see Subjects and Methods). The average age of uveitis patients was 49 years old and the majority were women (71%). Similar age and sex distribution were present in the control group (Table 1). In the uveitis group, the majority of patients had diagnoses of posterior uveitis (n = 40; 54.8%), but patients with anterior uveitis (n = 20; 27.4%) and intermediate (n = 8; 11.0%) and panuveitis (n = 5; 6.8%) were also represented.

• **CC FD ANALYSIS IN UVEITIS AND HEALTHY CONTROLS:** A total of 222 en face CC images were generated from the 3- × 3-mm and 6- × 6-mm scans of the 111 study eyes. Representative CC en face slabs from control subjects and uveitis subjects are shown in Figure 2. The FD maps for control subjects reveal numerous, small, relatively

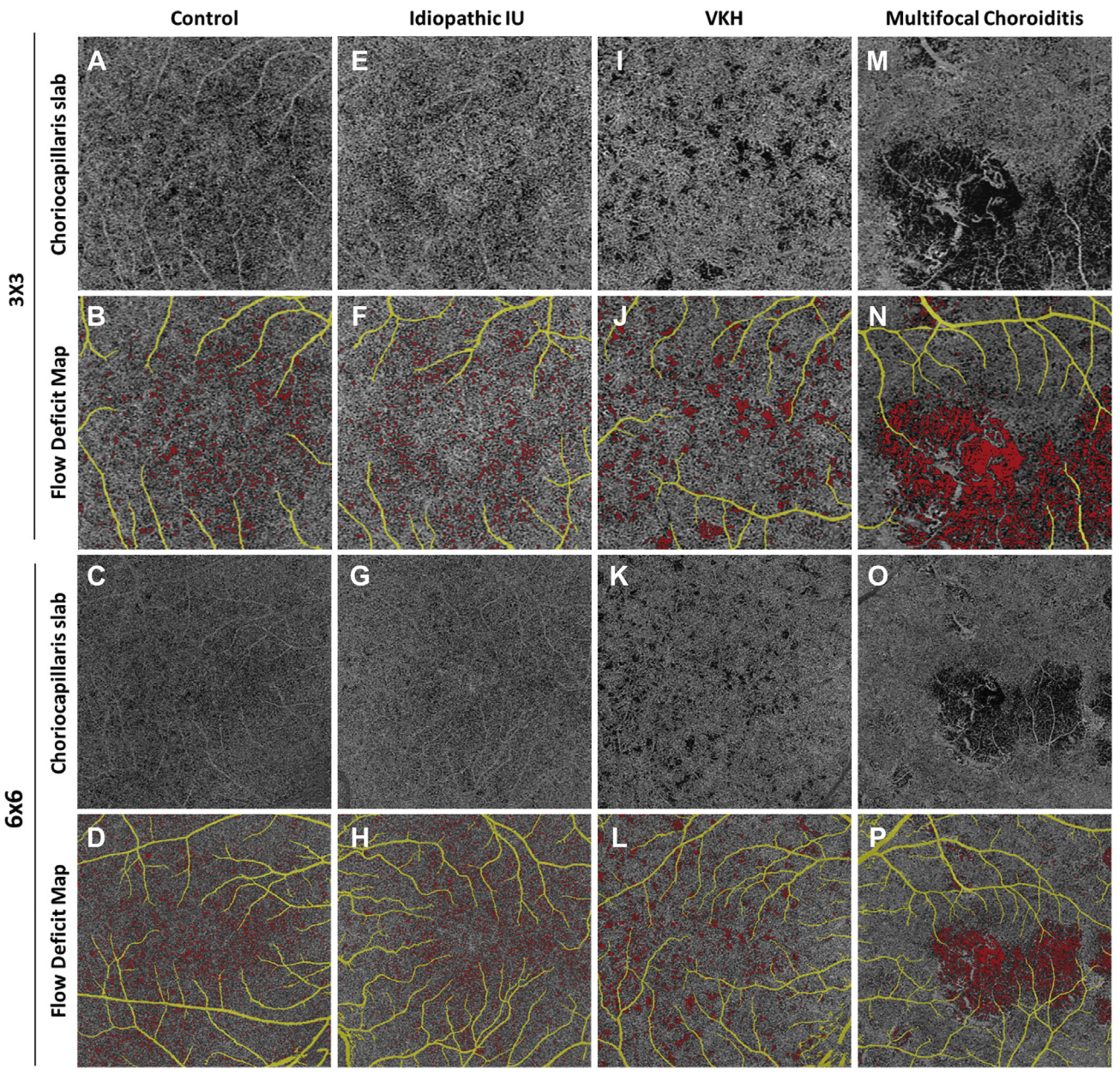

FIGURE 2. Automated detection of flow deficits (FDs) in control and uveitis. For uveitis, examples are idiopathic intermediate uveitis, Vogt-Koyanagi-Harada disease and multifocal choroiditis. (A, E, I, M) Optical coherence tomography angiography (OCTA) choriocapillaris (CC) slab in 3- × 3-mm scans. (B, F, J, N) Computed FD map in 3- × 3-mm scans, with FDs color coded in red, retinal projection artifacts color coded in yellow. (C, G, K, O) OCTA CC slab in 6- × 6-mm scans. (D, H, L, P) Computed FD map in 6- × 6-mmscans, with FDs color coded in red, retinal projection artifacts color coded in yellow.

evenly spaced FDs throughout the macula. Images from uveitis patients demonstrated a range of findings. For example, images from patients with anterior and intermediate uveitis lacked qualitative lesions and appeared similar to images from control subjects (Figure 2, E through H). In contrast, in patients with posterior uveitis, abnormalities of the FD map were grossly apparent. In a patient with Vogt-Koyanagi-Harada disease, multiple enlarged FDs can be appreciated on both the 3- × 3-mm and 6- × 6-mm images (Figure 2, I through L). An additional example is provided by a patient with multifocal choroiditis that demonstrates large areas of abnormal flow signal consistent with widespread loss of the CC (Figure 2, M through P).

To determine the differences between control and uveitic eyes quantitatively, the 3 CC flow metrics, FDN, MFDS and FDD, were compared between the control and uveitis groups. Prior to intergroup comparisons, metric repeatability was established by using a subset of both

TABLE 2. Intravisit Repeatability of Proposed Choriocapillaris Analysis

CV	FDN	MFDS (μm^2)	FDD
3 × 3 mm Control	5.06%	2.58%	4.17%
3 × 3 mm Uveitis	6.57%	5.57%	6.65%
6 × 6 mm Control	3.85%	1.29%	3.79%
6 × 6 mm Uveitis	5.00%	4.29%	4.72%

CV = coefficient of variation; FDD = flow deficit density; FDN = flow deficit number; MFDS = mean flow deficit size.

TABLE 3. Quantitative Analysis of Choriocapillaris Flow Metrics in Uveitis and Controls

	3 × 3 mm			6 × 6 mm		
Median (IQR)	FDN	MFDS (μm^2)	FDD	FDN	MFDS (μm^2)	FDD
Control	417 (123)	751.74 (69.64)	0.037 (0.008)	2365 (681)	802.02 (42.13)	0.058 (0.013)
Uveitis	442 (141)	838.36 (310.25)	0.042 (0.023)	2323 (829)	870.93 (274.14)	0.063 (0.018)
Mann-Whitney *U* test	$P = .1061$	$P < .0001$[a]	$P = .0002$[a]	$P = .6917$	$P < .0001$[a]	$P = .0076$[a]

FDD = flow deficit density; FDN = flow deficit number; IQR = interquartile range; MFDS = mean flow deficit size. IQR is the single number value for the range between Q3 and Q1.

[a]The result was significant after Bonferroni correction.

control and uveitis images. CVs ranged from 1.29% to 6.65% (Table 2), with MFDS having the lowest CV among the 3 metrics (Table 2). The summary of the results for each metric in the uveitis and normal control images are presented in Table 3. In control eyes, the median FDNs were 417 (Q_3-Q_1: 123) per 3- × 3-mm image and 2,365 (Q_3-Q_1: 681) per 6- × 6-mm image. No significant differences in FDN were identified between control and uveitis patients. In control subjects, the median MFDS was 751.7 μm^2 (IQR: 69.6 μm^2) per 3- × 3-mm image and 802.0 μm^2 (IQR: 42.1 μm^2) per 6- × 6-mm image. In uveitis images, the median MFDS was significantly larger than that of control subjects in both the 3- × 3-mm scans (median: 838.4 μm^2; IQR: 310.2 μm^2; $P < .0001$) and the 6- × 6-mm scans (median: 870.9 μm^2; IQR: 274.1 μm^2; $P < .0001$). Uveitis patients also demonstrated a significantly higher FDD than that in control subjects (3- × 3-mm scans, $P = .0002$; 6- × 6-mm scans, $P = .0076$). Thus, this analysis revealed that CC FDs were larger and more densely clustered in the uveitis patients than in control subjects.

• **UVEITIS SUBGROUP ANALYSIS:** To further investigate the presence of CC abnormality in different types of uveitis, the uveitis cohort was divided into 2 groups. Group A (n = 42) had no choroidal involvement, whereas group B (n = 31) showed choroidal involvement (Table 4).[42–45] Group A included diagnoses such as idiopathic anterior uveitis, HLA-B27-associated anterior uveitis, idiopathic intermediate uveitis, idiopathic anterior uveitis associated with multiple sclerosis, Fuch's heterochromic iridocyclitis, Possner-Schlossman syndrome, Susac syndrome, idiopathic retinal vasculitis, and autoimmune retinopathy. Group B subjects included diagnoses with choroidal involvement such as birdshot chorioretinopathy, multifocal choroiditis with and without panuveitis, punctate inner choroiditis, sarcoidosis, serpiginous choroiditis, panuveitis, ampiginous choroiditis and Vogt-Koyanagi-Harada disease. The 2 uveitis groups, A and B, were compared to each other and to normal control subjects.

After subdivision, the impact of the location of inflammation on quantitative parameters became apparent (Figure 3, Table 5). In uveitis group B (posterior and panuveitis), the median MFDS increased to 1,108 μm^2 on 3- × 3-mm images and to 1,104 μm^2 on 6- × 6-mm images. These values remained significantly larger than those in normal control subjects ($P < .0001$). Conversely, in the uveitis group A (anterior and intermediate uveitis), the MFDS decreased to 784 μm^2 on 3- × 3-mm images and to 820 μm^2 for 6- × 6-mm images. These values were no longer significantly different from those of control subjects ($P = .0339$ for 3- × 3-mm images; $P = .0239$ for 6- × 6-mm images; significant level a = .017 with Bonferroni correction). FDD was also significantly higher in uveitis group B than in uveitis group A and normal control subjects ($P < .0001$). FDNs were not significantly different between groups. In summary, these data show that uveitis patients with choroidal involvement have FDs that are both larger

TABLE 4. Subgroup of Uveitis Patients By Choroidal Involvement

Uveitis Without Choroidal Involvement (Group A)		Uveitis With Choroidal Involvement (Group B)	
n = 42 (Active = 14, 33%)		n = 31 (12, 39%)	
Idiopathic AU	12 (6)	Birdshot chorioretinopathy	13 (4)
Retinal vasculitis	9 (0)	Multifocal choroiditis	6 (1)
Idiopathic IU	7 (6)	Serpiginous choroiditis	4 (3)
Idiopathic IU associated with MS	1 (0)	Multifocal choroiditis and panuveitis	2 (1)
HLA-B27	6 (1)	Ampiginous choroiditis	1 (1)
Susac's syndrome	3 (0)	Punctate inner choroiditis	2 (0)
Autoimmune retinopathy	2 (1)	Vogt-Koyanagi-Harada disease	1 (1)
Fuchs iridocyclitis	1 (0)	Sarcoidosis	1 (1)
Posner-Schlossman syndrome	1 (0)	Panuveitis	1 (0)

The total number of patients per group is listed for each diagnosis. The number in parentheses indicates the number of patients with disease activity at the time of imaging.

AU = anterior uveitis; HLA-B27 = human leukocyte antigen-B27.

and more densely clustered than those in uveitis patients without choroidal involvement and normal control subjects. The number of scans obtained in patients with disease activity noted by the clinician on the date of imaging are also reported in Table 4. In total, 26 of the imaged patients (35%) had active uveitis (n = 14; 33% group A; and n = 12; 39% group B).

• **IMPACT OF SCAN PATTERN SIZE ON QUANTITATIVE CC ANALYSIS:** This study 2 scan patterns, 3- × 3-mm and 6- × 6-mm scans. For each scan pattern there is a different digital resolution and signal-to-noise ratio (SNR), which affects the quantitative results. The 3- × 3-mm scans provided a higher SNR (the 3- × 3-mm scan uses 4 repeated B-scans) and scanning density (10 μm/pixel) and may be more sensitive to small variations in FD size. The 6- × 6-mm scans provided access to larger regions of the posterior pole but at the cost of digital resolution (12 μm/pixel) and SNR (6- × 6-mm uses 2 repeated B-scans). To determine which scan size and quantitative parameter has the best ability to differentiate uveitis group B from control subjects, the AUC generated by the ROC was assessed for each possible combination of test and scan pattern (Figure 4). In both the 3- × 3-mm and the 6- × 6-mm images, MFDS could best differentiate uveitis group B from control subjects (3 × 3 mm: AUC = 0.9480; 6 × 6 mm: AUC = 0.9714). FDD also demonstrated good ability to discriminate using both scan sizes (3 × 3 mm: AUC = 0.8505; and 6 × 6 mm: AUC = 0.8093). FDN was not able to differentiate uveitis group B from control subjects in either 3- × 3-mm images (fail, AUC 0.5733) or 6- × 6-mm images (fail, AUC = 0.4429).

To further investigate the relationship between quantitative CC analyses in the 2 scanning sizes, parametric Spearman correlation tests were conducted for all 3 FD metrics (Figure 5). Significant correlation (all $P < .0001$) was observed for all 3 metrics, with MFDS demonstrating the strongest correlation among all (r = 0.8026) (Figure 5, C), followed by FDD (r = 0.5072) (Figure 5, A), and FDN (r = 0.388) (Figure 5, B). These results indicate that, although 3- × 3-mm scans and 6- × 6-mm scans have different discriminative powers, as demonstrated by the ROC data, each FD measurement is still significantly correlated and all are good at distinguishing uveitis group B from control subjects.

DISCUSSION

THIS STUDY USED A COMBINATION OF THE COMMERCIALLY available SS-OCTA en face CC images and a novel automated algorithm to automatically identify and quantify CC FDs in patients with uveitis. Using this unbiased, objective approach, it was found that the FDs in patients with uveitis are larger in size and occur at a higher density than FDs of normal control subjects. Furthermore, after subdividing the uveitis cohort into 2 groups based on the absence (uveitis group A) or presence (uveitis group b) of choroidal involvement, it was possible to refine the scope of the findings. Not surprisingly, the subgroup analysis found that, in the absence of known choroidal disease, CC FDs in uveitis patients were not significantly different from those in control subjects. In contrast, in patients with posterior or panuveitis, where the choroid is the main site of inflammation, CC FDs were significantly larger and presented with higher density than FDs in both normal control subjects and patients with anterior segment inflammation.

Quantitative analysis of CC blood flow presents different challenges than similar analyses of retinal vascular blood flow, including OCT signal attenuation, signal scattering though the RPE/BM complex, and the high degree of

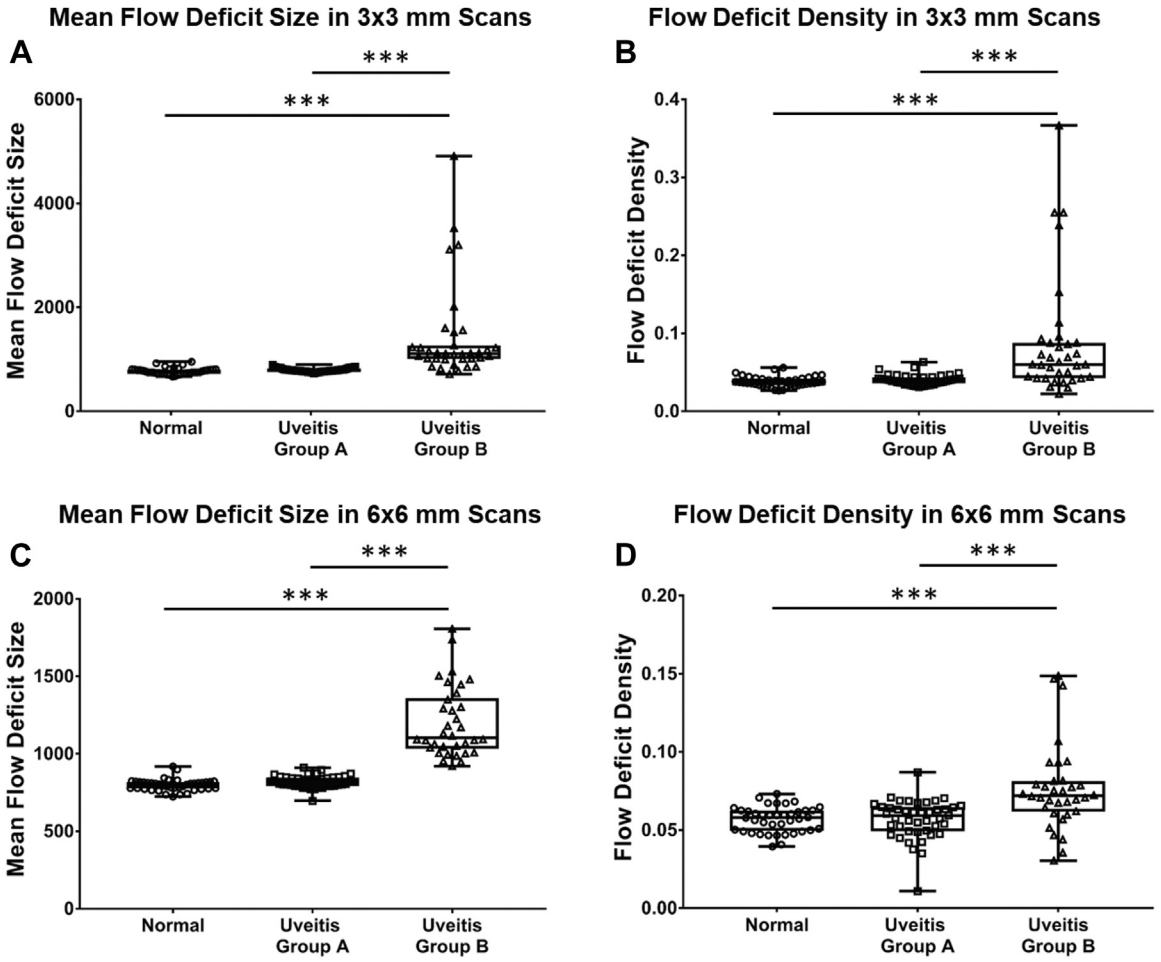

FIGURE 3. Scatter plot of flow deficit density (FDD) and mean flow deficit size (MFDS) in uveitis subgroups and control subjects in both 3- × 3-mm and 6- × 6-mm scans. (A) MFDS in 3- × 3-mm scans. (B) FDD in 3- × 3-mm scans. (C) MFDS in 6- × 6-mm scans. (D) FDD in 6- × 6-mm scans. ***$P < 0.0001$.

lateral resolution required to accurately resolve CC structure.[46] Moving from SD-OCTA to SS-OCTA has made choroidal anatomy more accessible and provides improved image quality for quantitative analysis, but high-quality, high- resolution images are still difficult to obtain. This study used a postacquisition image processing approach to address these on-going challenges. The approach used here consisted of a combination of complex thresholding that is sensitive to the intrinsic histogram of each image,[47] elimination of subphysiological size FDs,[34] structural compensation for possible signal attenuation due to RPE,[33] and removal of projection artifacts[40] to improve image quality and decrease interscan CV. The authors believe these postprocessing steps are necessary given the current stage of technology deployed in commercially available SS-OCTA systems. The results of this study indicate that this approach is useful and can produce results with good repeatability.

One of the benefits of quantitative image analysis is that it can provide an objective measurement of clinically relevant parameters of choroidal blood flow for longitudinal monitoring. Quantitative metrics of the retinal vasculature have been developed that describe the length, density, and branching patterns of the vessels, and these metrics have been used to define characteristics of the retinal vasculature in healthy and diseased eyes.[2–4,48,49] In contrast to the approach used to define retinal blood flow, terms defining CC blood flow have been developed that describe the areas without blood flow. This convention was adopted partially because normal CC vasculature cannot be completely resolved by commercial OCTA systems. Common OCTA lateral resolution (~15-20 μm) is larger than common CC intercapillary distance in the posterior pole (5-20 μm)[50] but smaller than the intercapillary distance in the retina (71.30 ± 5.17 μm).[51] Therefore, the most striking features in the CC en face images obtained from a normal eye are the small dark spots that represent the absence of detectable flow rather than the normal CC vasculature. In eyes with posterior segment pathology, the dark spots tend to match areas of pathology defined

TABLE 5. Quantitative Analysis of Choriocapillaris Flow Metrics in Patients With Uveitis Subgroups and Controls

	3 × 3 mm			6 × 6 mm		
Median (IQR)	FDN	MFDS (μm^2)	FDD	FDN	MFDS (μm^2)	FDD
Normal	417 (123)	751.7 (69.6)	0.037 (0.008)	2,365 (681)	802.0 (42.1)	0.058 (0.013)
Uveitis group A	446 (111)	784.6 (51.1)	0.040 (0.008)	2,391 (737)	820.9 (55.7)	0.059 (0.015)
Uveitis group B	438 (234)	1,108.4 (258.4)	0.060 (0.045)	2284 (1,251)	1,104.5 (328.1)	0.072 (0.020)
Kruskal-Wallis test (a = 0.05)	$P = .2666$	$P < .0001$[a]	$P < .0001$[a]	$P = .4680$	$P < .0001$[a]	$P < .0001$[a]
Mann-Whitney U test (a = .017)						
Control: Uveitis Group A	$P = .2041$	$P = .0339$	$P = .1428$	$P = .9144$	$P = .0239$	$P = .9357$
Control: Uveitis Group B	$P = .4366$	$P < .0001$[a]	$P < .0001$[a]	$P = .2348$	$P < .0001$[a]	$P < .0001$[a]
Uveitis Group A: Uveitis Group B	$P = .9608$	$P < .0001$[a]	$P < .0001$[a]	$P = .2028$	$P < .0001$[a]	$P < .0001$[a]

FDD = flow deficit density; FDN = flow deficit number; IQR = interquartile range; MFDS = mean flow deficit size. IQR is the single number value for the range between Q3 and Q1.

[a]The result was significant after Bonferroni correction.

by other standard of care clinical imaging modalities.[15,24] The terminology for these dark spots has not been firmly established, but they have been termed FDs, flow voids, or flow signal voids.[33–35,38,52] These authors favor the term FD as the OMAG[c] algorithm used to generate flow data is based on the movement of red blood cells. Thus, the absence of a flow signal most likely represents a deficit of red blood cell flow.

Use of 3 previously published quantitative metrics was chosen to summarize and compare the images in this study: total FDN, MFDS, and FDD.[53] It was found that patients with posterior uveitis had significantly larger MFDS and higher FDD than both the normal control subjects and uveitis patients without posterior involvement. Furthermore, this pattern held true for images from both the 3- × 3-mm scans and the 6- × 6-mm scans. Quantitative metrics that are robust when applied to high-resolution foveal scans, as well as larger size scanning patterns, will be important for use in diagnosing diseases such as uveitis that often have pathology extending throughout and beyond the central macula. Furthermore, the ROC analysis suggests that, although the 3- × 3-mm scans outperformed the 6- × 6-mm scans using FDD (3- × 3-mm scans: AUC = 0.8505; 6- × 6-mm scans: AUC = 0.8093), the 6- × 6-mm scans were better than the 3- × 3-mm scans for detecting pathology in patients with uveitis when using MFDS as the indicator of disease (3- × 3-mm scans: AUC = 0.9480; 6- × 6-mm: AUC = 0.9714). It is common that OCTA parameters calculated using different scan sizes result in different diagnostic powers.[54] These authors suspect one reason for the differences in this study is the size and location of CC pathology in relation to the area of the macula covered by the different area that is imaged. Some pathology was not contained within or could not be fully captured by the 3- × 3-mm scans. Another potential factor is the higher digital resolution of the 3- × 3-mm scans. The 3- × 3-mm OCTA images are generated using 4 repeated B-scans and have a lateral spacing of 10 μm/pixel. In contrast, 6- × 6-mm scans use 2 repeated B-scans to generate OCTA data with a lateral spacing of 12 μm/pixel. Thus, 3- × 3-mm scans may be more sensitive to small or subtle differences in FDs, whereas 6- × 6-mm scans are better at detecting pathology that generates less subtle (i.e., large) FD changes that are common in patients with posterior uveitis. Clinical examination will almost always be sufficient for diagnosing uveitis, and it is unlikely that CC FD metrics would be indicated as a diagnostic test. However, there are forms of posterior uveitis that mimic age-related macular degeneration, and it is possible that differences in MFDS could help differentiate less common causes of a choroidal neovascular membrane, like posterior placoid choroiditis or punctate inner choroiditis, from age-related macular degeneration.

In this study, the fully automated process of CC quantification followed the commercially available process and device-specific process for generating the CC OCTA image. Because this was a research-based proof of concept study, images generated by the device- specific software were not excluded if they had gross segmentation errors. Instead, the segmentation was corrected manually prior to quantitative analysis. Accurate CC slab generation using OCTA relies heavily on accurate identification of the RPE/BM complex. Although commercial systems perform well when segmenting healthy eyes, automated RPE segmentation in eyes with pathology at the level of the RPE can be more challenging.[55] Ultimately, for this approach to

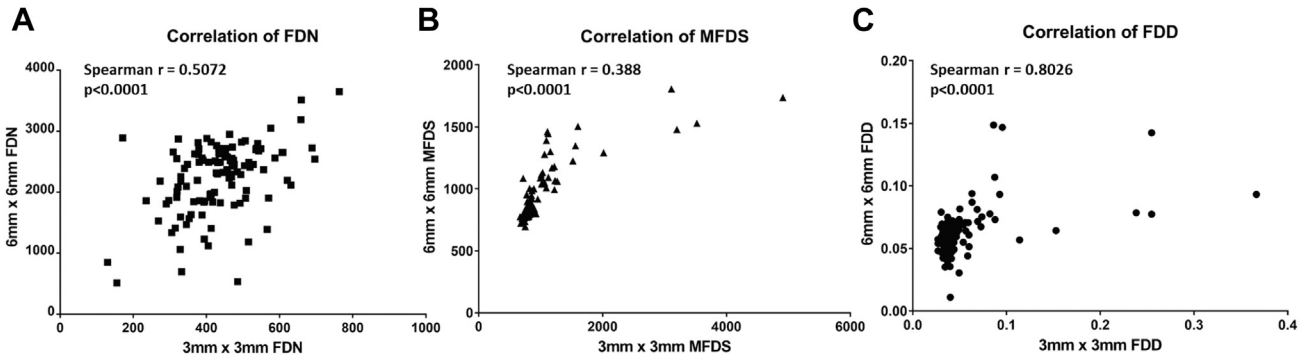

FIGURE 4. Nonparametric Spearman correlation of 3- × 3-mm and 6- × 6-mm scans for quantitative choriocapillaris metrics. (A) Spearman correlation of 3- × 3-mm and 6- × 6-mm scans with flow deficit number. (B) Spearman correlation of 3- × 3-mm and 6- × 6-mm scans with mean flow deficit size. (C) Spearman correlation of 3- × 3-mm and 6- × 6-mm scans with flow deficit density. FDN = flow deficit number; MFDS = mean flow deficit size.

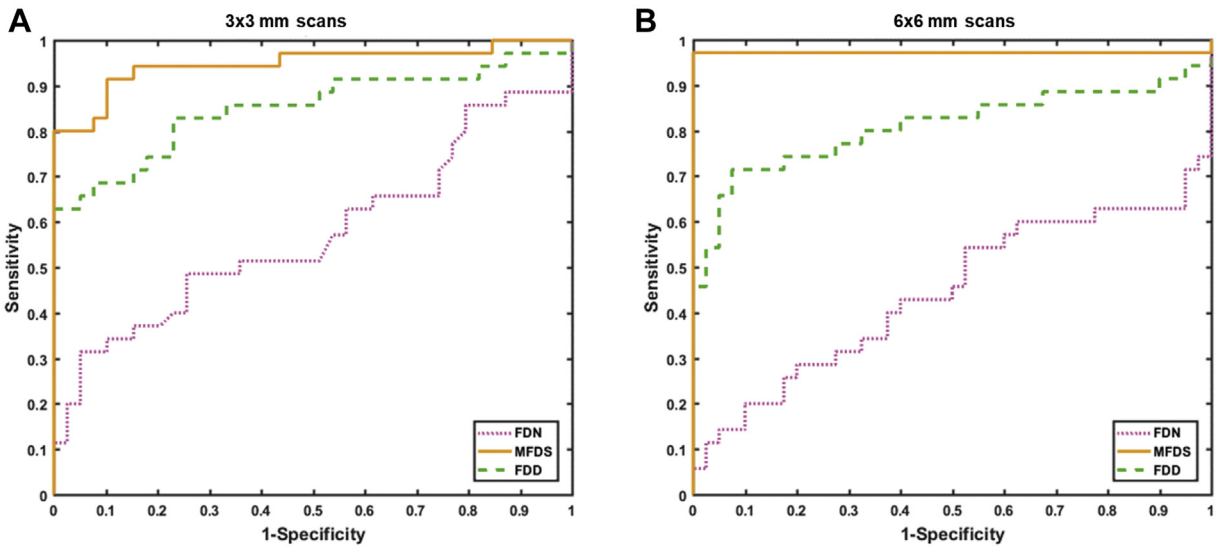

FIGURE 5. Receiver operating characteristic curves of all choriocapillaris quantitative metrics. (A) Receiver operating characteristic curves of all choriocapillaris quantitative metrics in 3- × 3-mm scans. (B) Receiver operating characteristic curves of all choriocapillaris quantitative metrics in 6- × 6-mm scans. FDN = flow deficit number; MFDS = mean flow deficit size; FDD = MFDS and flow deficit density.

become clinically accessible, it would require full and reliable automation at all stages of image acquisition and analyses. Optimization of segmentation performance in eyes with pathology at the level of the RPE is on-going and necessary for realization of the goal for fully automated analysis.

There are a number of limitations to this automated approach. Most importantly, signal strength has an impact on reproducibility of FD identification. A highly curated data set was used here that represented images with a signal strength of 8 or higher. Due to many possible causes of media opacity in patients with uveitis, these high-quality scans are not always achievable. However, this level of scan quality was achievable in 26 of the 31 active uveitis patients recruited to this study (5 who were imaged were excluded from the study). This success may not be typical because not all patients seen in clinic were sequentially recruited, and the success in imaging those patients is likely affected by selection bias. Also, this study was limited by the small number of patients imaged with each specific diagnosis. Due to the small sample size, the entire uveitis cohort was divided into 2 groups based on the presence or absence of choroidal involvement rather than on each individual diagnosis. This design allowed us to make conclusions about the performance of the automated image analysis approach in detecting the presence and extent of CC pathology but did not allow making disease-specific conclusions. Future studies with larger sample sizes are certainly warranted to determine the clinical relevance of this type of image analysis to specific forms of posterior

uveitis. Finally, the study cohort was cross-sectional and lacked longitudinal scans. Thus, an analysis to correlate disease activity with quantitative FD parameters was not performed. Despite these limitations, the study demonstrated that reliable, automated, quantitative CC assessment could identify significant differences in clinically distinct uveitis populations.

In summary, this study demonstrates that a fully automated image analysis process is reliable and can be used to generate unbiased quantitative metrics of CC pathology in eyes with posterior uveitis. This method for automated and quantitative analysis of CC FDs could be developed into a invasive clinical tool for monitoring patients with posterior uveitis.

ALL AUTHORS HAVE COMPLETED AND SUBMITTED THE ICMJE FORM FOR DISCLOSURE OF POTENTIAL CONFLICTS OF INTEREST and none were reported.

FUNDING/SUPPORT: Supported by National Eye Institute grants NEI K08EY023998, R01 EY024158, and R01 EY028753, Cynthia and Joseph Gensheimer Fellowship, Research to Prevent Blindness Career Development Award, Carl Zeiss Meditec, and an unrestricted Departmental Grant from Research to Prevent Blindness. The funding organization had no role in the design or conduct of this research.

FINANCIAL DISCLOSURES: R.K.W. has received research support from Carl Zeiss Meditec; holds intellectual property owned by Oregon Health and Science University and University of Washington; and he receives research support from Tasso, Moptim, Colgate Palmolive, and Facebook; and he is a consultant for Photonic Solutions, Kowa, and Carl Zeiss Meditec. All other authors have reported that they have no relationships relevant to the contents of this paper to disclose.

REFERENCES

1. Spaide RF, Klancnik JM, Cooney MJ. Retinal vascular layers imaged by fluorescein angiography and optical coherence tomography angiography. *JAMA Ophthalmol* 2015;133:45–50.
2. Koulisis N, Kim AY, Chu Z, et al. Quantitative microvascular analysis of retinal venous occlusions by spectral domain optical coherence tomography angiography. *PLoS One* 2017;12:e0176404.
3. Kim AY, Rodger DC, Shahidzadeh A, et al. Quantifying retinal microvascular changes in uveitis using spectral-domain optical coherence tomography angiography. *Am J Ophthalmol* 2016;171:101–112.
4. Kim AY, Chu Z, Shahidzadeh A, Wang RK, Puliafito CA, Kashani AH. Quantifying microvascular density and morphology in diabetic retinopathy using spectral-domain optical coherence tomography angiography quantifying vascular changes in DR with SD-OCTA. *Invest Ophthalmol Vis Sci* 2016;57:OCT362–OCT370.
5. Chu Z, Lin J, Gao C, et al. Quantitative assessment of the retinal microvasculature using optical coherence tomography angiography. *J Biomed Opt* 2016;21:066008.
6. Waizel M, Todorova MG, Terrada C, LeHoang P, Massamba N, Bodaghi B. Superficial and deep retinal foveal avascular zone OCTA findings of non-infectious anterior and posterior uveitis. *Graefes Arch Clin Exp Ophthalmol* 2018;256:1977–1984.
7. Spaide RF, Klancnik JM Jr, Cooney MJ. Retinal vascular layers in macular telangiectasia type 2 imaged by optical coherence tomographic angiography. *JAMA Ophthalmol* 2015;133:66–73.
8. Hwang TS, Jia Y, Gao SS, et al. Optical coherence tomography angiography features of diabetic retinopathy. *Retina* 2015;35:2371–2376.
9. Thorell MR, Zhang Q, Huang Y, et al. Swept-source OCT angiography of macular telangiectasia type 2. *Ophthalmic Surg Lasers Imaging Retina* 2014;45:369–380.
10. Hassan M, Agarwal A, Afridi R, et al. The role of optical coherence tomography angiography in the management of uveitis. *Int Ophthalmol Clin* 2016;56:1–24.
11. Talisa E, Bonini Filho MA, Adhi M, Duker JS. Retinal and choroidal vasculature in birdshot chorioretinopathy analyzed using spectral domain optical coherence tomography angiography. *Retina* 2015;35:2392–2399.
12. Khairallah M, Abroug N, Khochtali S, et al. Optical coherence tomography angiography in patients with Behcet uveitis. *Retina* 2017;37:1678–1691.
13. Pichi F, Sarraf D, Arepalli S, et al. The application of optical coherence tomography angiography in uveitis and inflammatory eye diseases. *Prog Retin Eye Res* 2017;59:178–201.
14. Graham E, Stanford M, Shilling J, Sanders M. Neovascularisation associated with posterior uveitis. *Br J Ophthalmol* 1987;71:826–833.
15. Pakzad-Vaezi K, Khaksari K, Chu Z, Van Gelder RN, Wang RK, Pepple KL. Swept-source OCT angiography of serpiginous choroiditis. *Ophthalmol Retina* 2018;2:712–719.
16. Howes EL, Cruse VK. The structural basis of altered vascular permeability following intraocular inflammation. *Arch Ophthalmol* 1978;96:1668–1676.
17. Nazari H, Hariri A, Hu Z, Ouyang Y, Sadda S, Rao NA. Choroidal atrophy and loss of choriocapillaris in convalescent stage of Vogt-Koyanagi-Harada disease: in vivo documentation. *J Ophthalmic Inflamm Infect* 2014;4–9.
18. Aggarwal K, Agarwal A, Mahajan S, et al. The role of optical coherence tomography angiography in the diagnosis and management of acute Vogt–Koyanagi–Harada Disease. *Ocul Immunol Inflamm* 2018;26:142–153.
19. Borrelli E, Souied EH, Freund KB, et al. Reduced choriocapillaris flow in eyes with type 3 neovascularization and age-related macular degeneration. *Retina* 2018;38:1968–1976.
20. Klufas MA, Phasukkijwatana N, Iafe NA, et al. Optical coherence tomography angiography reveals choriocapillaris flow reduction in placoid chorioretinitis. *Ophthalmol Retina* 2017;1:77–91.
21. Spaide RF. Choriocapillaris flow features follow a power law distribution: implications for characterization and mechanisms of disease progression. *Am J Ophthalmol* 2016;170:58–67.
22. Xu J, Song S, Men S, Wang RK. Long ranging swept-source optical coherence tomography-based angiography outperforms its spectral-domain counterpart in imaging human skin microcirculations. *J Biomed Opt* 2017;22:116007.

23. Zhang Q, Rezaei KA, Saraf SS, Chu Z, Wang F, Wang RK. Ultra-wide optical coherence tomography angiography in diabetic retinopathy. *Quant Imaging Med Surg* 2018;8:743–753.
24. Pepple KL, Chu Z, Weinstein J, Munk MR, Van Gelder RN, Wang RK. Use of en face swept-source optical coherence tomography angiography in identifying choroidal flow voids in 3 patients with birdshot chorioretinopathy. *JAMA Ophthalmol* 2018;136:1288–1292.
25. Cheung CMG, Yanagi Y, Mohla A, et al. Characterization and differentiation of polypoidal choroidal vasculopathy using swept source optical coherence tomography angiography. *Retina* 2017;37:1464–1474.
26. Jung JJ, Chen MH, Chung PY, Lee SS. Swept-source optical coherence tomography angiography for choroidal neovascularization after bevacizumab and photodynamic therapy. *Am J Ophthalmol Case Rep* 2016;1:1–4.
27. Byon I, Nassisi M, Borrelli E, Sadda SR. Impact of slab selection on quantification of choriocapillaris flow deficits by optical coherence tomography angiography. *Am J Ophthalmol* 2019;208:397–405.
28. Jabs DA, Nussenblatt RB, Rosenbaum JT, Standardization of Uveitis Nomenclature (SUN) Working Group. Standardization of uveitis nomenclature for reporting clinical data. Results of the First International Workshop. *Am J Ophthalmol* 2005;140:509–516.
29. Meditec CZ. Carl Zeiss Meditec Plex Elite 9000 OCT 501(k) premarket report of FDA 2016https://www.zeiss.com/meditec/int/product-portfolio/optical-coherence-tomography/plex-elite-9000-swept-source-oct.html#specifications. Accessed April 5, 2020.
30. Nassisi M, Shi Y, Fan W, et al. Choriocapillaris impairment around the atrophic lesions in patients with geographic atrophy: a swept-source optical coherence tomography angiography study. *Br J Ophthalmol* 2018;103:911–917.
31. Gorczynska I, Migacz J, Jonnal R, Zawadzki R, Poddar R, Werner J. Imaging of the human choroid with a 1.7 MHz A-scan rate FDML swept source OCT system. SPIE Digital Library. Available at: https://www.spiedigitallibrary.org/conference-proceedings-of-spie/10045/1004510/Imaging-of-the-human-choroid-with-a-17-MHz-A/10.1117/12.2251704.short?SSO = 1. Accessed June 14, 2020.
32. Wang RK. Optical microangiography: a label-free 3-D imaging technology to visualize and quantify blood circulations within tissue beds in vivo. *IEEE J Sel Top Quantum Electron* 2010;16:545–554.
33. Zhang Q, Zheng F, Motulsky EH, et al. A novel strategy for quantifying choriocapillaris flow voids using swept-source OCT Angiography. *Invest Ophthalmol Vis Sci* 2018;59:203–211.
34. Chu Z, Zhou H, Cheng Y, Zhang Q, Wang RK. Improving visualization and quantitative assessment of choriocapillaris with swept source OCTA through registration and averaging applicable to clinical systems. *Sci Rep* 2018;8:16826.
35. Zhang Q, Shi Y, Zhou H, et al. Accurate estimation of choriocapillaris flow deficits beyond normal intercapillary spacing with swept source OCT angiography. *Quant Imaging Med Surg* 2018;8:658–666.
36. Rochepeau C, Kodjikian L, Garcia M-A, et al. Optical coherence tomography angiography quantitative assessment of choriocapillaris blood flow in central serous chorioretinopathy. *Am J Ophthalmol* 2018;194:26–34.
37. Al-Sheikh M, Phasukkijwatana N, Dolz-Marco R, et al. Quantitative OCT angiography of the retinal microvasculature and the choriocapillaris in myopic eyes. *Invest Ophthalmol Vis Sci* 2017;58:2063–2069.
38. Zheng F, Zhang Q, Shi Y, et al. Age-dependent changes in the macular choriocapillaris of normal eyes imaged with swept-source optical coherence tomography angiography. *Am J Ophthalmol* 2019;200:110–122.
39. Spaide RF, Fujimoto JG, Waheed NK, Sadda SR, Staurenghi G. Optical coherence tomography angiography. *Prog Retin Eye Res* 2018;64:1–55.
40. Zhang Q, Zhang A, Lee CS, et al. Projection artifact removal improves visualization and quantitation of macular neovascularization imaged by optical coherence tomography angiography. *Ophthalmol Retina* 2017;1:124–136.
41. Bland JM, Altman DG. Measurement error proportional to the mean. *BMJ* 1996;313:106.
42. Cao JH, Silpa-Archa S, Freitas-Neto CA, Foster CS. Birdshot chorioretinitis lesions on indocyanine green angiography as an indicator of disease activity. *Retina* 2016;36:1751–1757.
43. Bouchenaki N, Cimino L, Auer C, Tran VT, Herbort CP. Assessment and classification of choroidal vasculitis in posterior uveitis using indocyanine green angiography. *Klin Monatsbl Augenheilkd* 2002;219:243–249.
44. Howe L, Stanford M, Graham E, Marshall J. Indocyanine green angiography in inflammatory eye disease. *Eye* 1998;12:761–767.
45. Rao NA. Pathology of Vogt-Koyanagi-Harada disease. *Int Ophthalmol* 2007;27:81–85.
46. Lauermann JL, Eter N, Alten F. Optical coherence tomography angiography offers new insights into choriocapillaris perfusion. *Ophthalmologica* 2018;239:74–84.
47. Wang Q, Chan S, Yang JY, et al. Vascular density in retina and choriocapillaris as measured by optical coherence tomography angiography. *Am J Ophthalmol* 2016;168:95–109.
48. Richter GM, Madi I, Chu Z, et al. Structural and functional associations of macular microcirculation in the ganglion cell-inner plexiform layer in glaucoma using optical coherence tomography angiography. *J Glaucoma* 2018;27:281–290.
49. Jia Y, Bailey ST, Hwang TS, et al. Quantitative optical coherence tomography angiography of vascular abnormalities in the living human eye. *Proc Natl Acad Sci U S A* 2015;112(18):E2395–E2402.
50. Olver J. Functional anatomy of the choroidal circulation: methyl methacrylate casting of human choroid. *Eye* 1990;4:262–272.
51. Chan G, Balaratnasingam C, Xu J, et al. In vivo optical imaging of human retinal capillary networks using speckle variance optical coherence tomography with quantitative clinicohistological correlation. *Microvasc Res* 2015;100:32–39.
52. Matet A, Daruich A, Hardy S, Behar-Cohen F. Patterns of choriocapillaris flow signal voids in central serous chorioretinopathy: an optical coherence tomography angiography study. *Retina* 2018;39:2178–2188.
53. Chu Z, Chen Y, Zhang Q, et al. Accurate visualization and quantification of choriocapillaris with swept source OCTA through averaging repeated volume scans. *Invest Ophthalmol Vis Sci* 2018;59:2880.
54. Chang R, Chu Z, Burkemper B, et al. Effect of scan size on glaucoma diagnostic performance using OCT angiography en face images of the radial peripapillary capillaries. *J Glaucoma* 2019;28:465–472.
55. Borrelli E, Shi Y, Uji A, et al. Topographic analysis of the choriocapillaris in intermediate age-related macular degeneration. *Am J Ophthalmol* 2018;196:34–43.